Lecture given at the 1980 Erice Course of the International School on Quantum Electronics on "Physics and Technology of Free Electron Lasers". To be published by Plenum Press, 227 West 17th Street, New York, NY 10011

BNL 28339

A THREE DIMENSIONAL CALCULATION OF ELECTRON ENERGY LOSS IN A VARIABLE PARAMETER FREE-ELECTRON LASER*

Alfredo Luccio and Claudio Pellegrini

Brookhaven National Laboratory

Upton, N.Y. 11973, U.S.A.

ABSTRACT

The motion of an electron beam through a longitudinally varying period undulator for a single-pass free-electron laser is studied. It is shown that, under certain conditions, the electrons are trapped in an optical "bucket", and deliver on the average more energy to the laser field than in constant period undulators of comparable parameters. The limits set by a finite beam emittance and energy spread are studied in detail by three-dimensional computer simulation.

I. INTRODUCTION

A single-pass free-electron laser (FEL) using a wiggler magnet with either the period, λ_w, and/or the magnetic field, B_w, varying along the magnet axis has been proposed recently.[1] The main advantage of this system over a "conventional" free-electron laser, having a constant period and magnetic field wiggler, is in the higher efficiency of the energy transfer from the electron beam to the laser radiation field. This efficiency, which is of the order of 1% in a conventional FEL, can be of the order of 30% in a variable wiggler FEL.

The theory of the variable wiggler FEL is based on a one dimensional model, in which the electron motion transverse to the laser axis is assumed to be given, and only the motion parallel to the axis is studied. In this paper, we want to study the effect on the laser efficiency of the electron transverse motion and evaluate the electron energy loss for a beam having a spread in angle and in the transverse position at the wiggler entrance.

* Work supported by the U.S. Department of Energy.

DISCLAIMER

The complete three dimensional equations of motion for an electron interacting with the laser field and the wiggler field are integrated numerically. We only consider the case of a small gain regime, assuming that the laser field intensity remains constant. We also limit ourselves to the case of a helical wiggler. The results are compared with the one dimensional model. The effect of the initial position and angular spread can, to a good approximation, be considered equivalent to an increase in the energy spread. the limits for this increased energy spread that must not be exceeded in order to avoid a loss in efficiency are nearly the same as in the one dimensional model.

II. THE EQUATIONS OF MOTION

To describe the energy exchange between the electrons and the radiation field, we use the single particle model developed by Colson.[2] We write the electron equations of motion in the wiggler field, B_w, and laser field, E_L, B_L, as

$$\frac{1}{c}\frac{d(\beta\gamma)}{dt} = \underline{E}_L^* + \underline{\beta} \times (\underline{B}_L^* + \underline{B}_w^*) \tag{1}$$

$$\frac{1}{c}\frac{d\gamma}{dt} = \underline{E}_L^* \cdot \underline{\beta} \tag{2}$$

where β is the electron velocity in units of the speed of light, c; γ is the electron energy in units of $m_o c^2$, the rest energy; the fields $\underline{E}^*$, $\underline{B}^*$ are normalized as

$$\underline{E}^* = e\,\underline{E}/(m_o c^2) \tag{3}$$

$$\underline{B}^* = e\,\underline{B}/(m_o c^2) \tag{4}$$

We decompose the velocity in a component, $\beta_{\parallel}$, parallel to the wiggler axis, z, and in the components β_x, β_y along the directions x, y orthogonal to the wiggler axis. We assume

$$\beta_{\parallel} \simeq 1;\ \beta_x,\ \beta_y << 1 \tag{5}$$

We use for the laser and the helical wiggler fields the following expressions

$$\underline{E}_L^* = E_L^* \left\{ \hat{x} \sin\left[\frac{2\pi}{\lambda}(z-ct) + \phi_o\right] + \hat{y} \cos\left[\frac{2\pi}{\lambda}(z-ct) + \phi_o\right] \right\} \tag{6}$$

$$\underline{B}_L^* = \hat{z} \times \underline{E}_L^* \tag{7}$$

$$\underline{B}_w^* = B_w^*(z) \left\{ \hat{x} \cos\phi_w + \hat{y} \sin\phi_w - \hat{z} \frac{2\pi}{\lambda_w} \left[x \sin\phi_w - y \cos\phi_w \right] \right\} \tag{8}$$

$$\phi_w = \int_o^z \{2\pi/\lambda_w(z')\}\, dz' \tag{9}$$

To write the wiggler field in the form (8) we have made the following assumptions:

i) the field intensity B_w^* and the period are slowly varying functions of z, so that

$$\frac{d\lambda_w}{dz} << 1; \quad \frac{\lambda_w}{B_w} \frac{dB_w}{dz} << 1;$$

we have neglected all terms containing these derivatives;

ii) we considered an expansion of the field in powers of x and y near to the wiggler axis, neglecting all terms quadratic or of higher order in $2\pi x/\lambda_w$, $2\pi y/\lambda_w$.

To determine the electron motion and energy change, we will use the equation (2) for γ and the equation (1) for β_x, β_y. The parallel velocity is then determined by the relationship

$$\beta_{\parallel} = \left[1 - \frac{1}{\gamma^2} - \beta_x^2 - \beta_y^2 \right]^{\frac{1}{2}} \tag{10}$$

For convenience we will use the variable

$$z = \int_o^t c\, \beta_{\parallel}(t')\, dt' \tag{11}$$

instead of t, the "polar" quantities

$$\beta_{\perp}\, e^{i(\alpha+\phi_w)} = \beta_x + i\beta_y \tag{12}$$

$$r\, e^{i\theta} = x + iy \tag{13}$$

and the relative phase of the electron and the radiation field

$$\phi = \frac{2\pi}{\lambda}(z-ct) + \phi_w + \phi_o \tag{14}$$

The complete set of equations can now be written as ($f' = \frac{df}{dz}$)

$$\gamma' = \frac{\beta_\perp E_L^*}{\beta_{\parallel}} \sin \phi \tag{15}$$

$$\phi' = \frac{2\pi}{\lambda_w} \left[1 - \frac{\lambda_w}{\lambda} \frac{1-\beta_{\parallel}}{\beta_{\parallel}} \right] + \alpha' \tag{16}$$

$$\beta_\perp' = \frac{2\pi K}{\lambda_w} \sin \alpha + \frac{1-\beta_{\parallel}-\beta_\perp}{\gamma\beta} E_L^* \sin \phi \tag{17}$$

$$\alpha' = \frac{2\pi}{\lambda_w} \left[\frac{K}{\gamma\beta_\perp} \cos \alpha - 1 \right] + \frac{K}{\gamma\beta_{\parallel}} \left(\frac{2\pi}{\lambda_w}\right)^2 r \sin (\phi_w - \theta) + \frac{1-\beta_{\parallel}}{\gamma\beta_\perp\beta_{\parallel}} E_L^* \cos \phi \tag{18}$$

$$r' = \frac{\beta_\perp}{\beta_{\parallel}} \cos (\phi_w + \alpha - \theta) \tag{19}$$

$$r\theta' = \frac{\beta_\perp}{\beta_{\parallel}} \sin(\phi_w + \alpha - \theta) \tag{20}$$

with

$$K = B_w^* \lambda_w / 2\pi \tag{21}$$

III. REDUCTION TO THE ONE DIMENSIONAL MODEL

We have solved the system of equations (15) to (21) by numerical integration. It is, however, useful to reduce the system to the form used in the one dimensional model and to describe briefly some of the main results obtained from it.

equations of the one dimensional model are obtained if one assumes

$$\beta_\perp' = 0, \qquad \beta_\perp = \frac{K}{\gamma} = \text{constant} \tag{22}$$

$$\alpha' = 0, \qquad \alpha = 0 \tag{23}$$

In this case, the particle trajectory is a helix of pitch angle $\beta_\perp$ and radius $\rho = \beta_\perp \lambda_w / 2\pi$.[3]

Using (10) we have

$$\beta_{\parallel} = \left[1 - \frac{1+K^2}{\gamma^2} \right]^{\frac{1}{2}} \simeq 1 - \frac{1+K^2}{2\gamma^2} \tag{24}$$

and from (15), (16)

$$\gamma' = \frac{KE_L^*}{\gamma} \sin\phi \tag{25}$$

$$\phi' = \frac{2\pi}{\lambda_w} \left[1 - \frac{\lambda_w}{\lambda} \frac{1+K^2}{2\gamma^2} \right] \tag{26}$$

Following reference (1) we define a resonant energy

$$\gamma_r^2 = \lambda_w (1+K^2)/2\lambda \tag{27}$$

and a synchronous phase, ϕ_r

$$\sin\phi_r = \frac{d\gamma_r^2}{dz} /2\,K E_L^* \tag{28}$$

The particles inside the "optical bucket" of width $(\Delta\phi, \Delta\gamma)$ will oscillate around ϕ_r, γ_r, and their average energy variation will be equal to the change in γ_r. In the following, we assume that the change in γ_r is due to a change in λ_w while K remains a constant. For a wiggler of length L_w, one obtains

$$\gamma_r^2(L_w) - \gamma_r^2(0) = 2\,K E_L^* L_w \tag{29}$$

The efficiency is then defined as

$$\eta = \frac{\gamma_r(0) - \gamma_r(L_w)}{\gamma_r(0)} \frac{\Delta\phi}{2\pi} \tag{30}$$

having assumed that the initial distribution of the phase is uniform in the interval $0-2\pi$. Assuming ϕ_r to be in the interval

π, $\frac{3}{2}\pi$, we have

$$\Delta\phi = 3\pi - \phi_r - \phi^* \tag{31}$$

where ϕ^* is a solution of the equation

$$V(\phi^*) = V(3\pi - \phi_r) \tag{32}$$

with

$$V(\phi) = \cos\phi + \phi \sin\phi_r \tag{33}$$

The bucket "height"

$$\Delta\gamma_B = \gamma - \gamma_r$$

is given by

$$\left(\frac{\Delta\gamma}{\gamma}\right)_B = \left[\frac{E_L^* K \lambda_w}{2\pi\gamma_r^2}\right]^{\frac{1}{2}} \{V(3\pi - \phi_r) - V(\phi_r)\}^{\frac{1}{2}} \tag{34}$$

Notice that in the case K= constant, the quantity $(\Delta\gamma/\gamma_r)$ is independent of z.

All these results are valid for particles injected with initial velocity $\beta_{xo} = K/\gamma$, $\beta_{yo} = 0$, and on axis. For particles injected off axis, the motion will be a superposition of the helical motion and an oscillation of reduced wavelength[3]

$$\lambda_f = \sqrt{2}\,\gamma\,\lambda_w/2\pi K$$

The amplitude of this oscillation is equal to the initial displacement r, for a particle injected off axis, or to $\sqrt{2}\,\gamma\,\lambda_w\,\Delta\beta/2\pi K$ for a particle injected at an angle. A particle executing this oscillation will experience a different magnetic field from a particle on axis

$$\frac{\Delta B_w}{B_w} = \frac{1}{2}\left(\frac{2\pi}{\lambda_w}\right)^2\left[r_o^2 + \left(\frac{\gamma\,\lambda_w}{\sqrt{2}\,\pi K}\,\Delta\beta_\perp\right)^2\right] \tag{35}$$

The change in B_w is equivalent to a change in K and hence to a change in r

$$\left(\frac{\Delta\gamma}{\gamma}\right)_{eff} = \frac{K^2}{1+K^2}\,\frac{\Delta K}{K} \tag{36}$$

and, using (35)

$$\left(\frac{\Delta\gamma}{\gamma}\right)_{eff} = \frac{K^2}{1+K^2}\ \frac{1}{2}\left(\frac{2\pi}{\lambda_w}\right)^2\left[r_o^2 + \left(\frac{\lambda_w}{\sqrt{2}\pi K}\Delta\beta_\perp\right)^2\right] \tag{37}$$

If the electron beam has an energy spread $\Delta\gamma/\gamma$, we can define a total energy spread

$$\left(\frac{\Delta\gamma}{\gamma}\right)_T = \left[\left(\frac{\Delta\gamma}{\gamma}\right)^2 + \left(\frac{\Delta\gamma}{\gamma}\right)^2_{eff}\right]^{1/2} \tag{38}$$

and assume that when the condition

$$\left(\frac{\Delta\gamma}{\gamma}\right)_T < \left(\frac{\Delta\gamma}{\gamma}\right)_B \tag{39}$$

is satisfied, the efficiency is still given to a good approximation by (34).

The validity of this assumption can be tested comparing (34) with the results obtained from the numerical integration of (15) to (21). This will be done in the next section.

Before closing this section, we notice that introducing the transverse electron beam emittance

$$\varepsilon = \pi\, r\, \Delta\beta \tag{40}$$

and assuming that the electron beam has cylindrical symmetry, we can rewrite (37) as

$$\left(\frac{\Delta\gamma}{\gamma}\right)_{eff} = \frac{1}{2}\left(\frac{2\pi}{\lambda_w}\right)^2 \frac{K^2}{1+K}\left[r^2 + \left(\frac{\gamma\lambda_w}{\sqrt{2}\pi^2 K}\right)^2 \frac{\varepsilon^2}{r^2}\right] \tag{41}$$

IV. NUMERICAL RESULTS

The Eqs. (15) through (21) have been integrated numerically, for various initial values of the quantities γ, ϕ, $\beta_\perp$, α, and r. The wiggler wavelength λ_w was assumed to vary linearly along the (helical) wiggler according to

$$\lambda_w = \lambda_{wo}\ (1 - z/\sigma) \tag{42}$$

With this, and from the definition of Eq. (28), the resonant phase angle becomes

$$\phi_r = \arcsin\left[\frac{-\lambda_{wo}}{2\sigma\lambda\varepsilon_o}\right] \tag{43}$$

A set of the free-electron laser parameters chosen for the calculations is shown in Table 1.

Table 1. Free-electron Laser Parameters

Wiggler wavelength (initial)	$\lambda_{wo} = 2$ cm
Wiggler overall length	$L_w = 2.5$ m
Wiggler taper length {Eq. (42)}	$\sigma = 5$ m
Wiggler parameter {Eq. (21)}	$K = 1$
Radiation wavelength	$\lambda = 10$ μm
Resonant "energy" {Eq. (27)}	$\gamma_{ro} = 44.733$
Normalized rad. field {Eq. (3)}	$E_L^* = 341\ m^{-1}$

As already mentioned in Sect. III, if the electrons are injected into the wiggler at a radius given by[2]

$$r_o = x_o = \lambda_{wo}^2/4\pi^2\rho_o \tag{44}$$

where $\rho_o = m_o\gamma_o c/eB_o$ is the cyclotron radius in the field B_o, and with a transverse velocity given by (22), (23), they move along a helical path close to the wiggler axis.

Figures 1 and 2 show a set of calculated curves of the energy γ vs. distance z along the wiggler in the two cases of $\sigma = 5$ m and 15 m, for a monochromatic bundle of 16 electrons with initial energy equal to the resonant energy; $\gamma_o = \gamma_{ro}$, injected exactly on the helical path defined by Eqs. (22), (23), (44), and with 16 equidistant starting phases ϕ_o between 0 and 2π.

Here, the resonant energy γ_r decreases with z according to

$$\gamma_r = \gamma_{ro}\sqrt{\lambda_w/\lambda_{wo}} \tag{45}$$

The capture of some of the electrons in an energy-phase bucket around γ_r shows clearly.

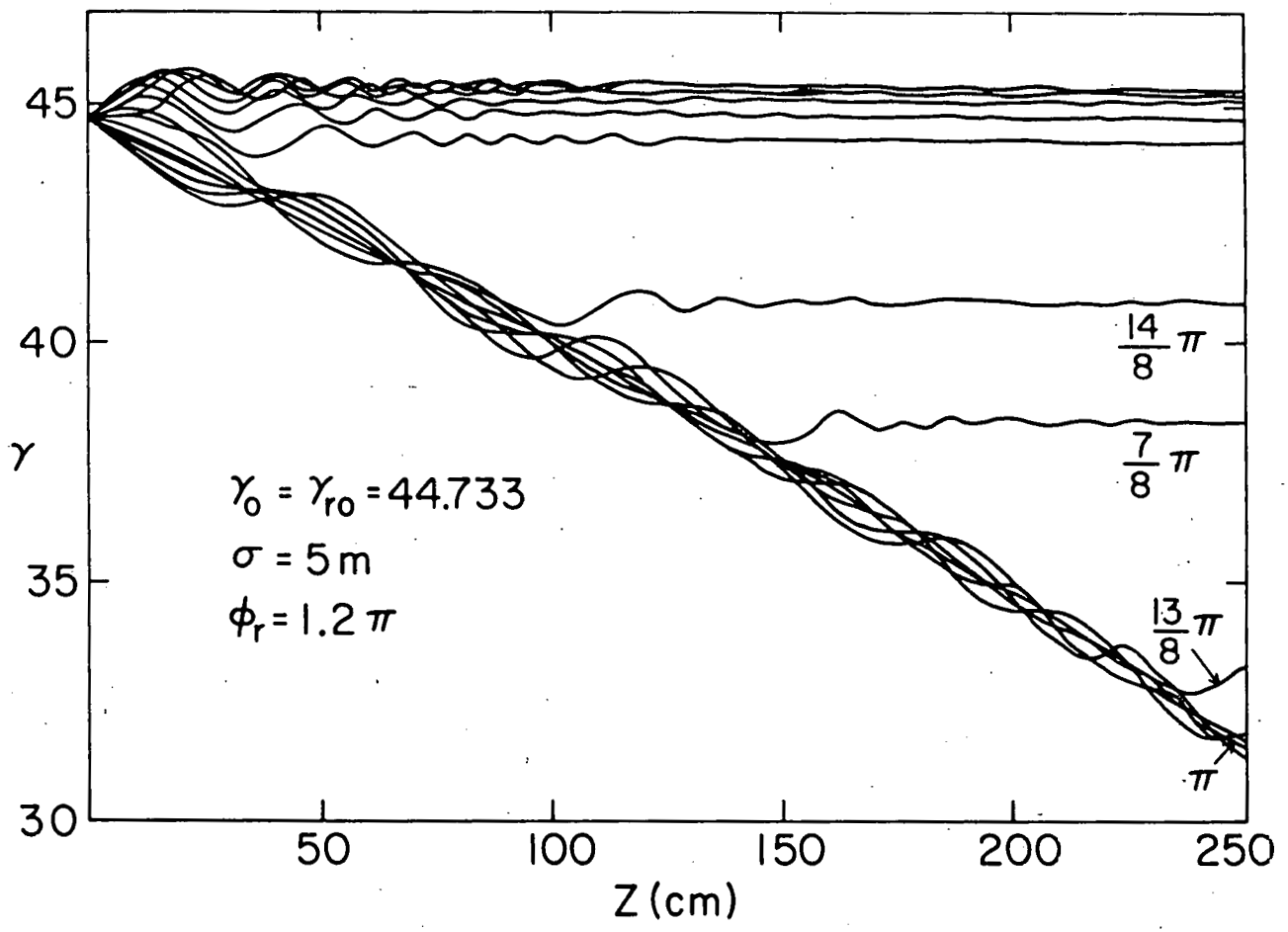

Fig. 1. Normalized energy γ vs. distance z along the wiggler. Monochromatic electron bundle with $\gamma_0 = \gamma_{ro} = 44.733$ injected on helix. Case σ = 5m.

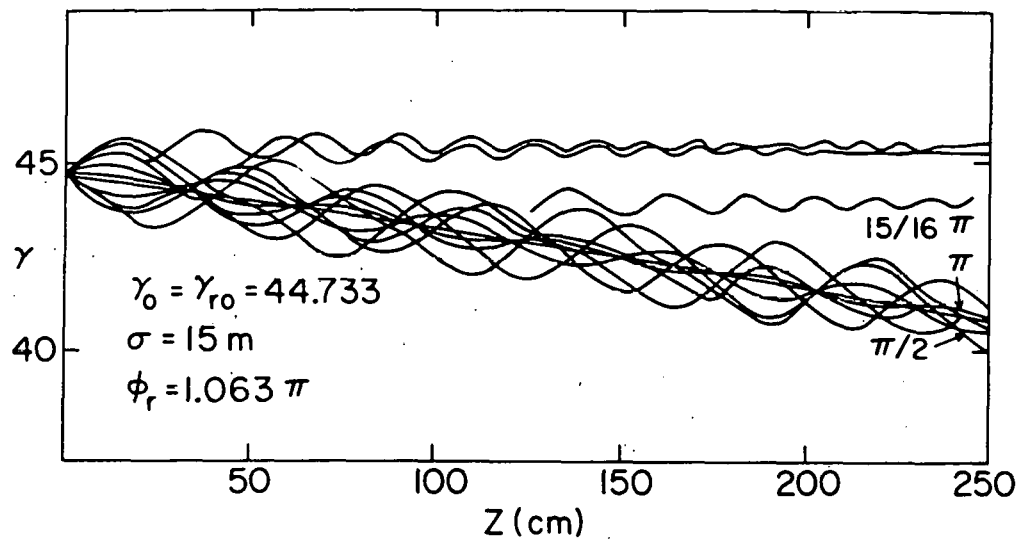

Fig. 2. Normalized energy γ vs. distance z along the wiggler. Monochromatic electron bundle with $\gamma_o = \gamma_{ro} = 44.733$ injected on helix. Case σ = 15 m.

Figures 3 and 4 show the trajectories of the representative points of the electrons in phase-space for the same cases. Here, the values of bucket parameters, from Eq. (43) and from Eqs. (31), (34), given in Table 2, appear to agree well with the numerical results. However, both the bucket height and width shown in Figs. 3, 4 are of the order of 10% smaller than the theoretical values.

Table 2. Phase Space Bucket Parameters

	σ	=	5 m	15 m
Resonant "energy"	γ_{ro}	=	44.733	
Resonant phase	ϕ_r	=	$1.200\,\pi$	$1.063\,\pi$
Energy height of bucket	$\left(\frac{\Delta\gamma}{\gamma_r}\right)_B$	=	1.63%	2.78%
Limit angles for bucket	ϕ^*	=	$0.867\,\pi$	$0.475\,\pi$
	$3\pi-\phi_r$	=	$1.800\,\pi$	$1.937\,\pi$
Phase width of bucket	$\Delta\phi$	=	$0.933\,\pi$	$1.462\,\pi$
Efficiency Eq. (30)	η	=	13.7%	6.4%

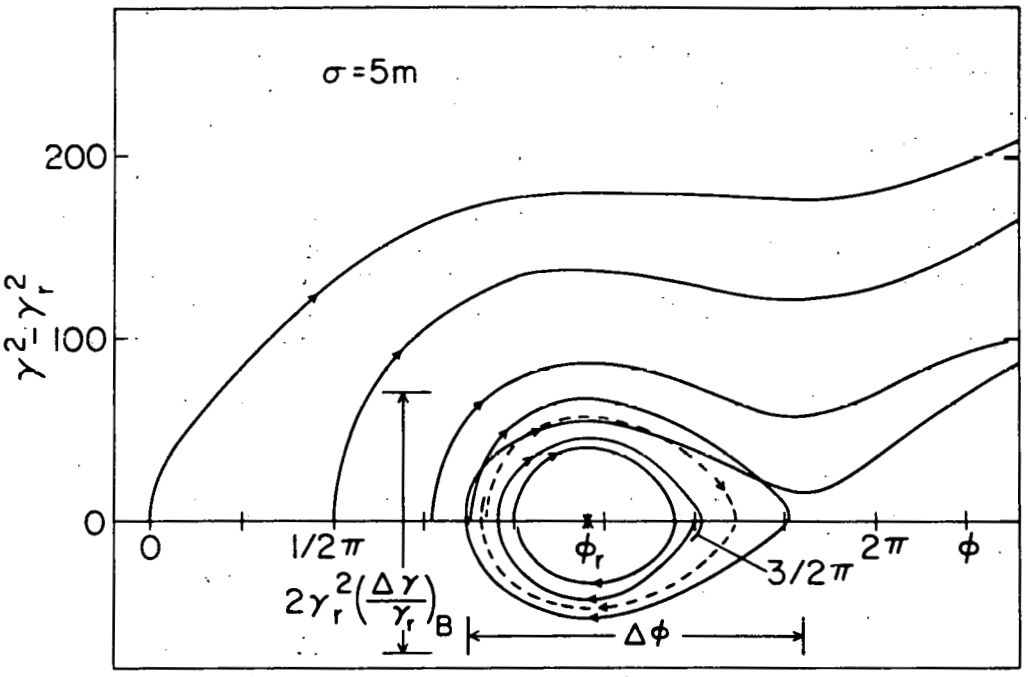

Fig. 3. Phase space trajectories of electrons injected on a helix. σ = 5 m. The capture width appears somewhat smaller than Δφ shown (see Table 2).

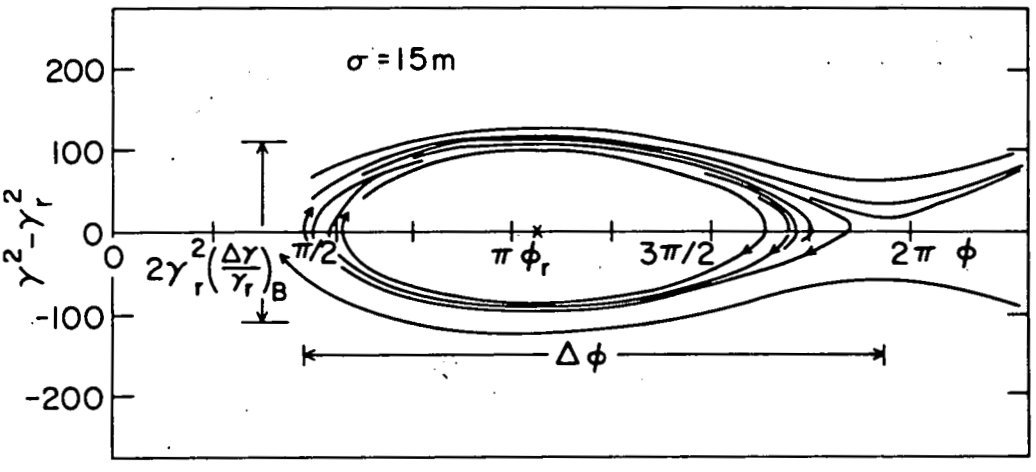

Fig. 4. Phase-space trajectories of electrons injected on a helix. Case σ = 15 m.

Once established the conditions for capture and energy loss of paraxial electrons with resonant energy, we moved on to find how a real beam, with finite emittance, behaves. As it has been shown in Sect. III, a finite radius of the beam and a transverse velocity spread around the values given by Eqs. (44), (22), (23), should act as an additional energy spread.

In our calculations, we assigned a parabolic shape to the density distribution of the beam in the γ, r, $\beta_\perp$ and α spaces, while the density in phase ϕ was always taken as uniform. To reduce the number of cases, we limited ourselves to consider separately the γ, r, $\beta_\perp$ and α sections of the four-dimensional phase space density volume.

Results for σ = 5 m are shown in Figs. 5 through 8.

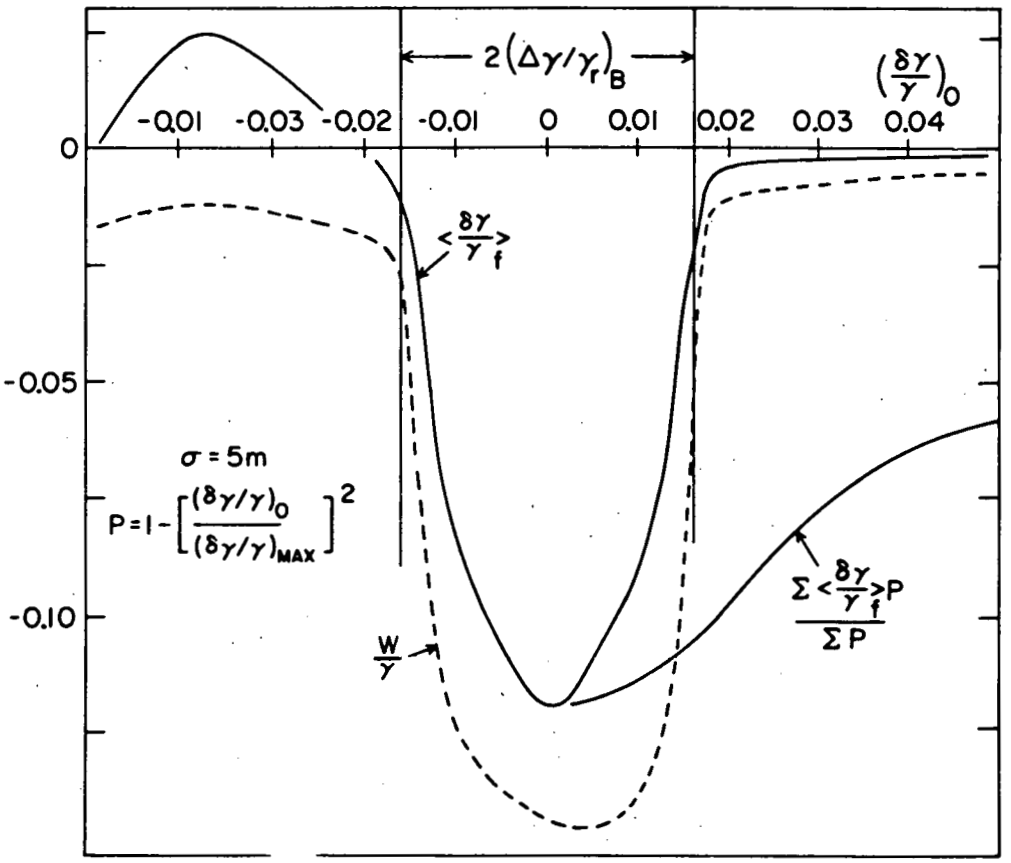

Fig. 5. Average energy loss $\langle\delta\gamma/\gamma\rangle$, relative statistical standard deviation W/γ and weighted average energy loss as a function of the initial energy. Electrons injected on helix. σ = 5 m. For comparison, the "height" of the bucket from Table 2 is also shown.

Figure 5 shows the average (respect to the initial phase, ϕ) energy loss $\langle \delta\gamma/\gamma \rangle$ and its statistical standard deviation W, as a function of the initial energy.

The bucket effective height, defined at the half maximum point, obtained from Fig. 5 is $(\Delta\gamma/\gamma_o) \simeq 1.31\%$. This value is almost 20% smaller than the value $(\Delta\gamma/\gamma)_B$ given in Table 2. Correspondingly, the maximum energy transfer, averaged over the phase, is 12% instead of the value of 13.4% given in the Table.

The values of W show also a pronounced peak within the bucket, where, because of the capture mechanism, the statistical distribution of final energies exhibits two well separated maxima.

In the same Fig. 5, we give also the average energy loss, weighted on a parabola. This shows that in the present case, a paraxial

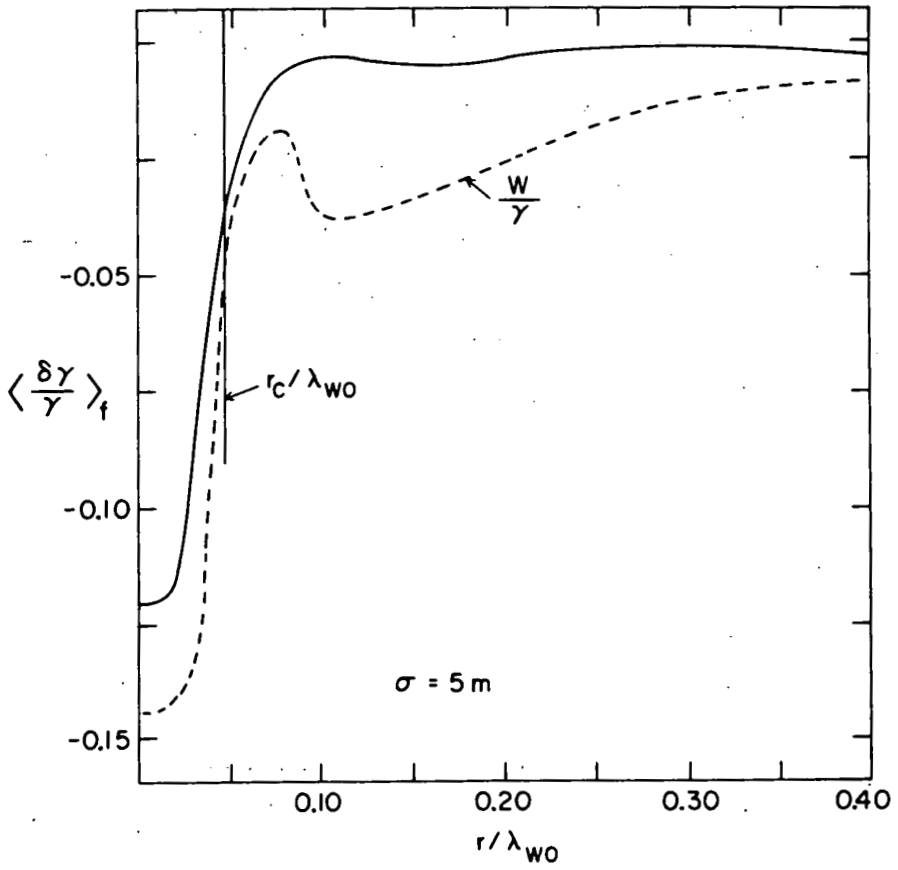

Fig. 6. Average energy loss $\langle \delta\gamma/\gamma \rangle$ and relative statistical standard deviation W/γ as a function of initial radius, for $\beta_{1_o} = K/\gamma$ and $\gamma_o = \gamma_{ro}$. σ = 5 m. The "capture" radius is also shown for comparison.

beam with 5% initial energy spread loses still on the average 6% of its energy to the radiation field. If the initial energy spread is equal to $(\Delta\gamma/\gamma_r)_B$, the average energy loss is only reduced from 12% to 11%.

Figure 6 shows analogous results for a beam with finite radial extension. According to Eq. (37), a spread in radius is equivalent to a spread in energy

$$\left.\frac{\Delta\gamma}{\gamma}\right|_{rad} = \frac{1}{2}\,\frac{K^2}{1+K^2}\left(\frac{2\pi r}{\lambda_w}\right)^2 \tag{46}$$

which gives, by assuming $\Delta\gamma/\gamma = 1.63\%$, a limiting value

$$r_{capt}/\lambda_w = 0.0406$$

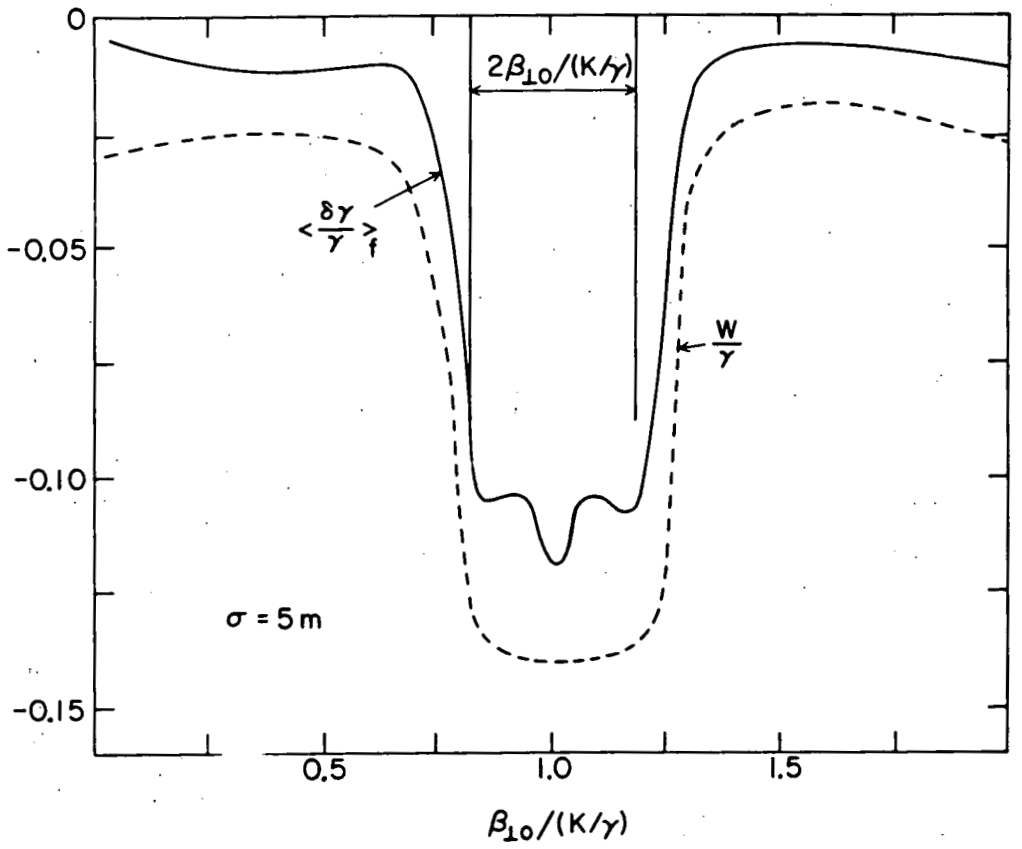

Fig. 7. Average energy loss $\langle\delta\gamma/\gamma\rangle$ and relative statistical standard deviation W/γ as a function of the initial transverse velocity, for $x_o = r_o$ and $\gamma_o = \gamma_{ro}$. $\sigma = 5$ m. The "capture transverse angle" is also shown.

in good agreement with the results.

Figures 7 and 8 show the effect of a transverse velocity dispersion around the values (22), (23). From Eq. (37) it appears that the limiting value for capture of $\beta_{\perp}$ equals the ratio of r_{capt} to the reduced wavelength of the long wavelength oscillations of the electron trajectories in the wiggler.

Hence

$$\beta_{\perp\,capt} = \frac{K}{\gamma} \pm \frac{r_{capt}}{\lambda_f} = \left(1 \pm \frac{2\pi}{\sqrt{2}} \frac{r_{capt}}{\lambda_w}\right) \cdot \frac{K}{\gamma} \tag{47}$$

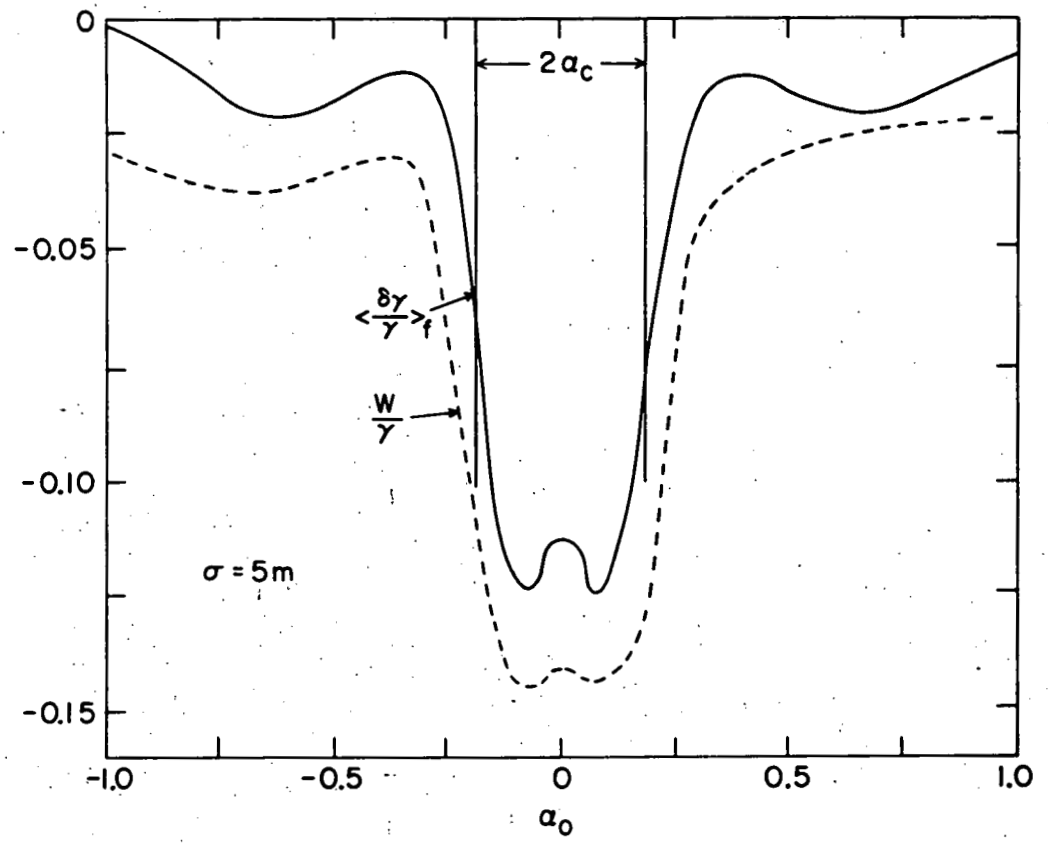

Fig. 8. Average energy loss $\langle \delta\gamma/\gamma \rangle$ and relative statistical standard deviation W/γ as a function of initial slant angle α_o, for $x_o = r_o$ and $\beta_{\perp o} = K/\gamma.\sigma = 5$ m. α_{capt} is also shown.

and, with the present values,

$$\beta_{\perp,capt} / (K/\gamma) = 1 \pm 0.180$$

again in good agreement with the results.

The same holds for the angle α that the vector $\beta_\perp$ makes with the tangent to the ideal paraxial helix. Limits for α , when $\beta_{\perp_o} = K/\gamma_o$, are

$$\alpha_{capt} = \pm \frac{2\pi}{\sqrt{2}} \frac{r_{capt}}{\lambda_w} = \pm 0.180$$

and they appear to bound well the calculated capture peak.

Both Figs. 7 and 8 show a fine structure in the behaviour of $\Delta\gamma/\gamma$ vs. $\beta_\perp$ and vs. α. They are not surprising since we did not

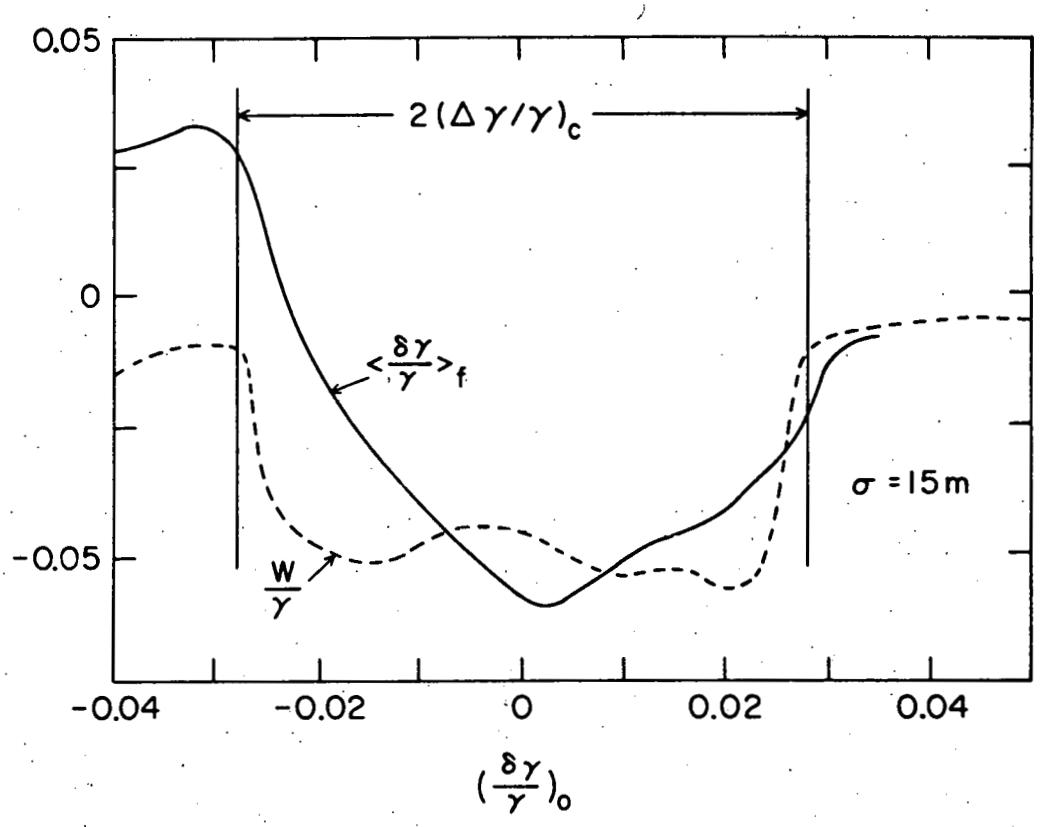

Fig. 9. Average energy loss $\langle\delta\gamma/\gamma\rangle$ and relative standard deviation W/γ as a function of initial electron energy. σ = 15 m.

average the results over the complete phase-space emittance of the electron beam, but limited ourselves to representative points on the axes. No systematic study of this fine structure was made.

Results of the numerical calculations for the case σ = 15 m are shown in Figures 9 through 12.

Figure 9 shows $\langle \delta\gamma/\gamma \rangle$ and W/γ as a function of the initial electron energy, for electrons injected exactly on a helix. In the figure, the value of the capture energy spread ("height of the bucket") from Table 2

$$\left(\frac{\Delta\gamma}{\gamma_r}\right)_B = \pm 2.78\%$$

is also shown.

Figures 10 and 11 show $\langle \delta\gamma/\gamma \rangle$ and W/γ as a function of r_o and

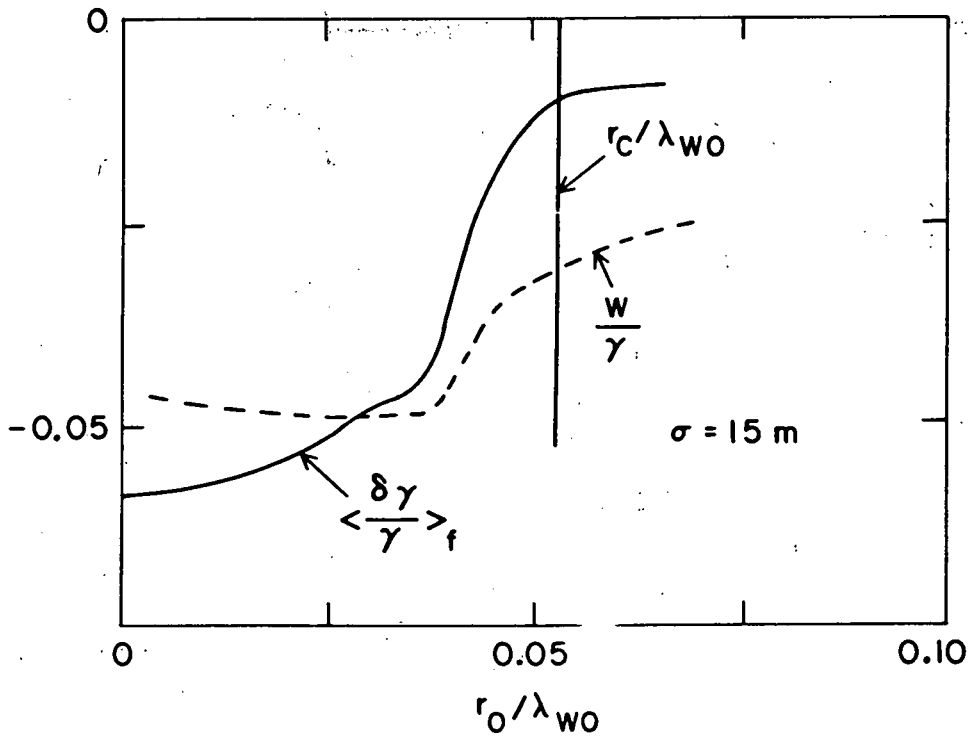

Fig. 10. Average energy loss $\langle \delta\gamma/\gamma \rangle$ and W/γ as a function of injection radius. σ = 15 m.

$\beta_{\perp o}$ respectively, with their capture ranges

$$r_c/\lambda_{wo} = 0.053$$

$$\left(\frac{\beta_{\perp_o}}{K/\gamma}\right)_c - 1 = \pm\ 0.234$$

Outside these ranges, the calculations gave as result oscillations in $\langle\delta\gamma/\gamma\rangle$ as large as 3%. However, by averaging over starting points on the phase-space ellipses

$$\left(\frac{2\pi r}{\lambda_{wo}}\right)^2 + \frac{\gamma^2}{K^2}(\Delta\beta_{\perp_o})^2 = \text{const} \qquad (49)$$

the $\langle\delta\gamma/\gamma\rangle$ was reduced to 0.8%.

Figure 12 shows $\langle\delta\gamma/\gamma\rangle$ and W/γ as a function of the slant angle α_o. Capture range for α is also shown.

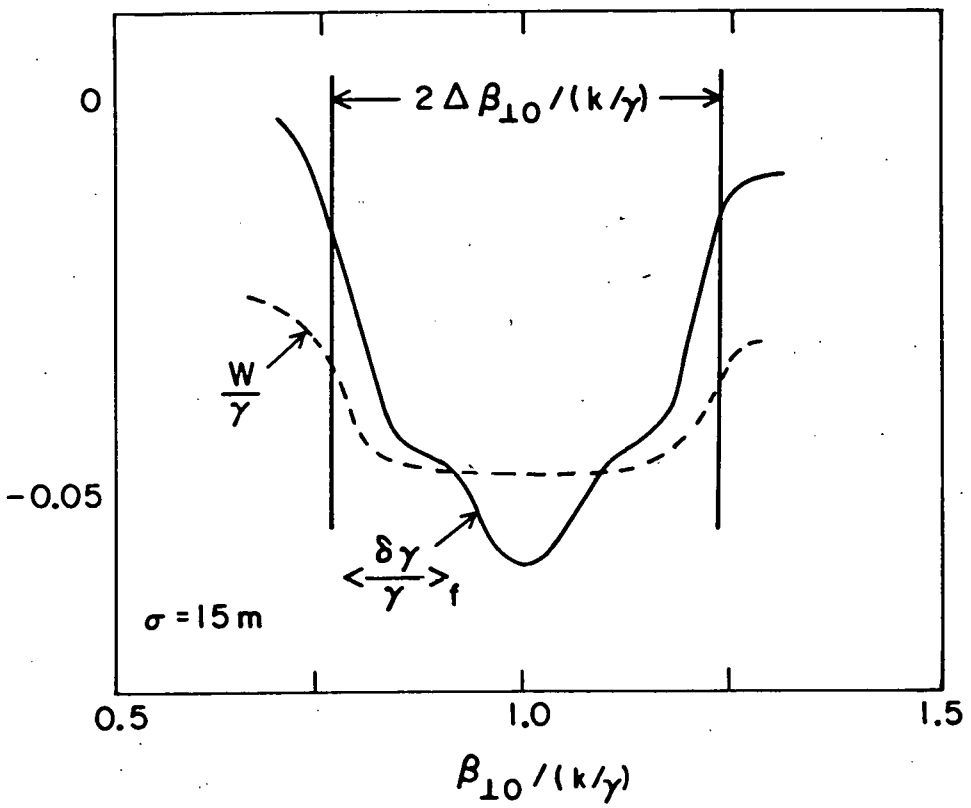

Fig. 11. Average energy loss $\langle\delta\gamma/\gamma\rangle$ and standard deviation W/γ as function of initial transverse velocity $\beta_{\perp_o}$. σ = 15 m.

REFERENCES

1. N.M. Kroll, P.L. Morton, and M.N. Rosenbluth,"Physics of Quantum Electronics", Vol. 7, Chap. 4, Addison-Wesley Publ. Co., (1980).
2. W.B. Colson, Phys. Letters, A59:187 (1976).
3. J.P. Blewett and R. Chasman, J. Appl. Phys., 48:2692 (1977).

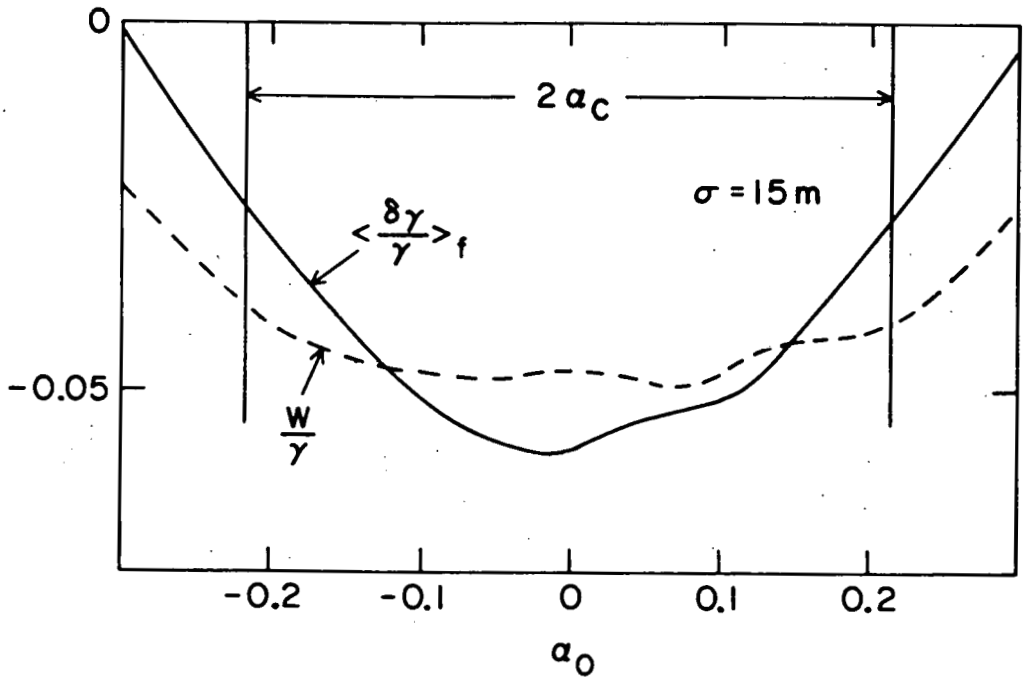

Fig. 12. Average energy loss $\langle \delta\gamma/\gamma \rangle$ and standard deviation W/γ as a function of initial slant angle α_o. σ = 15 m.